Available online at www.sciencedirect.com
ScienceDirect
Ceramics International 37 (2011) 1401–1407
CERAMICS INTERNATIONAL
www.elsevier.com/locate/ceramint

Phase stability and microstructure evolution of yttria-stabilized zirconia during firing in a reducing atmosphere

Chang-Ju Ho, Wei-Hsing Tuan *

Dept. of Materials Science & Engineering, National Taiwan University, Taipei 106, Taiwan

Received 22 September 2010; received in revised form 1 December 2010; accepted 4 January 2011
Available online 3 February 2011

Abstract

The phase transition and microstructure evolution of yttria-stabilized zirconia (YSZ) when firing in a reducing atmosphere are investigated in the present study. As the sintering temperature is lower than 1400 °C, the phase observed for the YSZ specimens is the first tetragonal (t) phase with a grain size of only 0.4 μm in average. When the sintering temperature is increased above 1450 °C, the second tetragonal (t′) phase appears together with a rapid grain growth rate. A surface layer with grains larger than 20 μm is observed for the YSZ specimens sintered at 1600 °C. It is found that the addition of metallic nickel particles has little influence on the phase transition of YSZ; however, the growth of t′-phase grains is reduced with the addition of Ni particles.

Keywords: A. Grain growth; Zirconia; Phase transformation; Reducing atmosphere

1. Introduction

The mechanical properties of yttria-stabilized zirconia (YSZ) are superior among ceramics. Apart from structural applications, YSZ has been used for many areas, such as the thermal barrier coating (TBC) for gas turbine blades [1] and the ionic conductor for solid oxide fuel cell (SOFC) [2] etc. Both zirconia coating and ionic conductor are operated in severe conditions involving heat and reducing environment. For example, the use of zirconia coating allows the increase of the operation temperatures to above 1300 °C [3]. The oxygen partial pressure within engine is very low due to the combustion of fuel. Furthermore, some residual carbon may be formed as a result of incomplete burning of fuel. For SOFC, the zirconia electrolyte is operated at an intermediate temperature in both oxidizing and reducing atmospheres. As carbon-containing fuel (such as methane) is used, residual carbon may also be formed [4–6]. The presence of carbon may generate a reducing atmosphere at elevated temperature.

There are three major polymorphs, monoclinic (m) tetragonal (t) and cubic (c) phases for zirconia. The stress-induced phase transformation from t to m is the origin for the high toughness of partial stabilized zirconia [7]. Apart from m, t and c phases, several other phases have also been found. For examples, an orthorhombic phase has been observed as an external pressure of 50 GPa was applied [8]. A rhombohedral phase was found sometime on the machined surface [9]. A second tetragonal phase, t′ phase, was often observed in the samples fast-cooled from c-phase region [10]. The t′ phase was also found in a 3 mol% Y_2O_3 doped ZrO_2 after sintering in N_2 at 1500–1650 °C [11]. Miller and his coworkers suggested that the transition from c phase to t′ phase was a diffusionless process [12]. Heuer and his colleagues looked into the microstructure of t′ phase and claimed that the c to t′ transformation was a displacive transformation [10,13,14]. The t′ phase was relatively stable against external pressure [15], the phase was thus a preferred phase for the TBC material [12]. Chevalier et al. also pointed out that the presence of t′ phase improves the low temperature degradation problem of YSZ [16]. The XRD patterns for t, c and t′ phases are very similar to each other. Nevertheless, the presence of t′ phase can be identified by using the X-ray diffraction (XRD) technique in the 2θ range from 72° to 76° [17–19].

The addition of aliovalent oxides, such as CaO, MgO, Y_2O_3 etc., reduces the martensite transformation starting temperature (Ms) to a temperature below room temperature [7]. The high

* Corresponding author. Tel.: +886 2 33663899; fax: +886 2 23659800.
E-mail address: tuan@ntu.edu.tw (W.-H. Tuan).

0272-8842/$36.00
doi:10.1016/j.ceramint.2011.01.008

temperature phase, such as t phase, thus remains till room temperature. The solution of these stabilizers is accompanied with the formation of oxygen vacancy to fulfill the neutrality requirement. The amount of oxygen vacancy may thus affect the phase stability of YSZ [20]. Besides using the stabilizers, the oxygen vacancy can also be created by heat-treating zirconia in an oxygen-lean environment. For examples, the solution of nitrogen into zirconia [11,19,21,22] and the use of flowing hydrogen [23] and carbon monoxide [24] can induce extra oxygen vacancy. In view of the applications for TBC and SOFC, the phase stability of YSZ in a reducing environment is an important issue.

The phase stability of zirconia is also affected by its microstructure. Among all the microstructure features, the grain size plays a critical role on the phase transformation ability. Spontaneous t to m transformation is taken place as the grain size of t-phase exceeds a threshold value (e.g. ~1 μm for 3 mol% Y_2O_3 doped ZrO_2) [25]. To control the grain growth behaviour of zirconia is a key issue for the application of t-phase zirconia. The growth of t-zirconia grains is relatively slow [26]. However, the grain growth rate of cubic phase is fast; a 30–250 faster growth rate, comparing to that of t-phase, has been reported [27]. The addition of a second phase particles may otherwise slow down the grain growth rate [28]. The grain growth behaviour of t′ phase has not been reported before. The transformation ability of t′ as a function of grain size has not been determined either.

For both SOFC and TBC applications, the zirconia and carbon may co-exist at elevated temperature. The presence of carbon may lower significantly the oxygen partial pressure at elevated temperature; a highly reducing atmosphere is thus resulted. The effect of the reducing atmosphere on the phase transition and microstructure evolution of ZrO_2 at elevated temperatures has attracted little attention. In the present study, the YSZ specimens are fired within a graphite powder bed, their phase transition and microstructure evolution during sintering are investigated. Furthermore, for the application of SOFC, metallic Ni particles are usually added into zirconia to act as the conductor for electrons. The effect of metallic particles on the phase transition and microstructure stability is also investigated.

2. Experimental procedures

A 3 mol% Y_2O_3-doped ZrO_2 powder (TZ-3Y, Tosoh Co., Japan) was used as the starting powder in the present study. Disc-shaped green compacts were prepared by uniaxial pressing the starting powder at 13 MPa. The sintering was carried out at 1400–1600 °C for 1 h. The heating rate and cooling rate were 5 °C/min. The sintering was carried out by burying the green compact in a graphite powder bed and cushioned on a graphite plate in a covered crucible. For comparison purpose, some specimens were prepared by sintering in air.

The effect of Ni particles on the phase and microstructure stability of YSZ in the reducing atmosphere was also investigated. The powder mixture of YSZ and Ni was prepared by using a chemical adsorption technique [29]. A nickel nitrate (Showa Chemicals Inc., Tokyo, Japan) solution was used to coat the nickel ions onto the zirconia powder. The nano-sized Ni particles were produced by heat-treating the coated powder in air and subsequently reduced in hydrogen. The resulting nickel content was determined by using an inductively coupled plasma-atomic emission spectrum (ICP-AES, Model 3000DV, Perkin Elmer, Optima, USA).

The sintered density was determined by using the Archimedes method with distilled water as the immersion medium. The X-ray diffraction (XRD, model TTRAXIII, Rigaku, Tokyo, Japan,) was used for phase analysis with CuKα radiation. The voltage and current used for XRD analysis were 50 kV and 300 mA. The phase analysis was conducted in the 2θ range from 20° to 80° with steps of 0.03° for 1.5 s, from 27° to 32° and from 72° to 76° with steps of 0.005° for 3 s. No surface grinding was applied before the phase analysis.

Before microstructure observation, the cross section of the specimens was obtained by cutting, grinding and polishing. The grain boundaries were revealed by thermal etching at 100 °C below the sintering temperature for 1 h. Both the scanning electron microscopy (SEM, XL30, Philip Co., Netherlands) or field-emission scanning electron microscopy (FE-SEM, Leo 1530, Philips Co. Netherlands) were used to characterize the microstructure. The grain size was calculated by using the line intercept technique on SEM photographs. More than 300 grains were counted. The quantitative analysis of yttrium distribution was performed by using an electron probe microanalysis (EPMA, Model JAX-8200, JOEL, Japan). The amount of yttria content was calibrated by using an air-sintered (1500 °C/1 h) specimen as the standard.

3. Results

The color of the YSZ specimens sintered in air is ivory; however, the color of the specimens sintered in CO is dark gray to black on the surface region and light gray inside. The change of color for zirconia specimens after sintering in a reducing atmosphere had also been reported in previous studies [19,23]. The reducing atmosphere used in the present study is generated by firing the specimens within a graphite powder bed. The specimens and graphite powder are first arranged in a covered alumina crucible, then fired to elevated temperatures in air. The amount of graphite powder is sufficiently large enough to cover the specimens even after firing at elevated temperature. The sintering atmosphere was mainly composing of a carbon monoxide, CO, and a very small amount of oxygen. The oxygen partial pressure in the atmosphere during sintering at 1400–1600 °C is very low, $\sim 10^{-17}$–10^{-16} atm, assuming that the thermodynamic equilibrium is achieved [30].

For the Ni-doped YSZ specimens, the amount of Ni in the YSZ–Ni powder mixture as determined by ICP-AES is 0.7 wt%, which corresponds to 0.6 vol% Ni. The color of the Ni-doped specimens after sintering in CO is black.

Fig. 1 shows the density of YSZ specimens and YSZ/Ni composites as a function of sintering temperature. The YSZ specimens reach their full density as they are sintered above

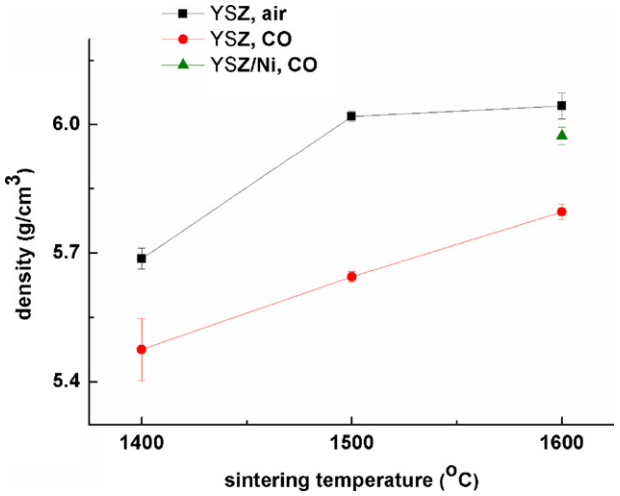

Fig. 1. Density of YSZ specimens and YSZ/Ni composites as a function of sintering temperature.

1500 °C in air. However, the density of YSZ specimens is relatively low as they are sintered within the graphite powder bed. The addition of Ni particles enhances the sintering activity of YSZ specimens in the reducing atmosphere.

Fig. 2 shows the microstructure of the YSZ specimens after sintering in air and in CO. The micrographs are all taken near the surface region of the specimens. The size of the ZrO_2 grains in the specimens sintered in air is smaller than 1 μm, even when the sintering temperature is as high as 1600 °C, Fig. 2(a). The grain size in the specimen sintered at 1400 °C in CO is also small, Fig. 2(b). A bimodal size distribution for the ZrO_2 grains is found in the specimen sintered at 1500 °C in CO, Fig. 2(c). The average size of the ZrO_2 grains is 1.5 μm, with larger grains around 2 μm and the smaller ones less than 0.5 μm. A surface layer composing of only coarse grains is observed in the YSZ specimens sintered at 1600 °C in CO, Fig. 2(d). The grain size decreases with the increase of the distance from the surface. Furthermore, the pore size also decreases with the increase of the distance from the surface. Some cracks along the grain boundary are also observed in the surface region.

Fig. 3(a) shows the fracture surface of the YSZ specimen sintered at 1600 °C in CO. Large grains with size >20 μm are observed near the surface; however, the size of the grains within the specimen remains small. The fracture surface of the YSZ/Ni composite after sintering at 1600 °C in CO is shown in Fig. 3(b). For the composite, the average size of ZrO_2 grains is around 6.6 μm at the surface region, 0.87 μm inside. Though the size difference is not as significant as that for the YSZ specimens sintered in CO, a grain size gradient is still observed for the YSZ/Ni specimen.

Fig. 4 shows the size of ZrO_2 grains in the YSZ specimens and YSZ/Ni composites after sintering in CO at various temperatures. The size of ZrO_2 grains for the specimen sintered in air is also shown for comparison. The ZrO_2 grains in the specimens sintered in air are the smallest. The ZrO_2 grains in the interior of the YSZ specimens sintered in CO are also small. However, the ZrO_2 grains near surface are large as the specimens are sintered above 1500 °C in CO. The addition of nickel particles reduces the size of ZrO_2 grains near the surface.

Fig. 5 shows the XRD patterns of the specimens after sintering. No surface grinding is applied before the XRD analysis. For all the specimens sintered in air and in CO, with or without the addition of Ni particles, their XRD patterns are very similar, Fig. 5(a). The XRD patterns in the 2θ range from 27° to 32° are the same for all the specimens, Fig. 5(b). It is worth noting that the amount of m phase is extremely low, at least below the detection limit. The presence of t′ phase can be identified only in the 2θ range from 72° to 76°, Fig. 5(c). The major phase for the YSZ specimens sintered in air is the first tetragonal (t) phase. A very small amount of c phase is found in the YSZ specimens sintered at 1500 °C in air. A small hump is

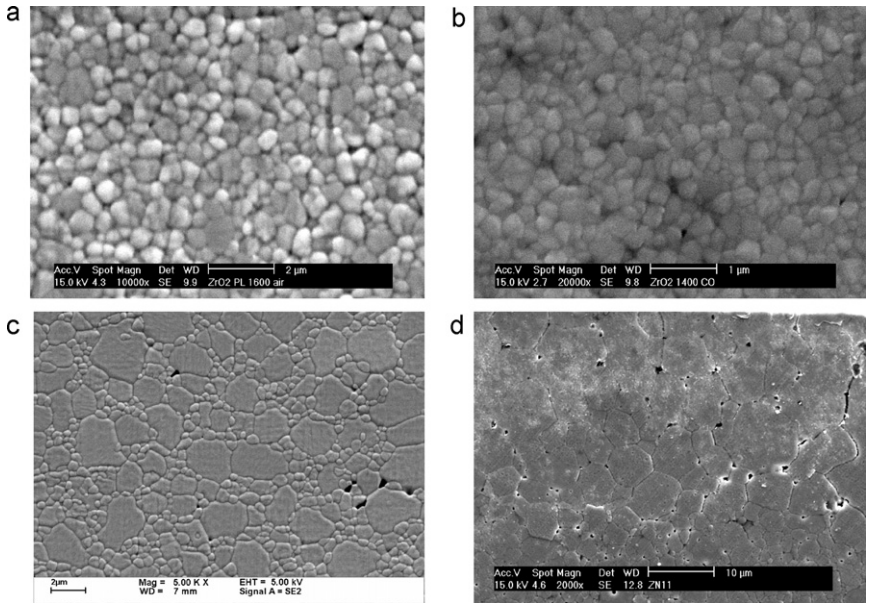

Fig. 2. Microstructures of the specimens sintered at (a) 1600 °C in air, and at (b) 1400 °C, (c) 1500 °C, (d) 1600 °C in CO.

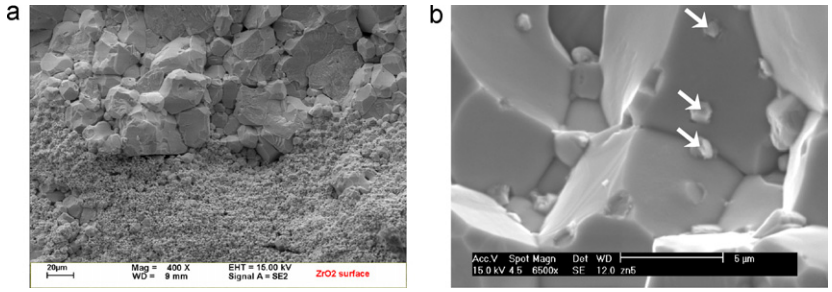

Fig. 3. Microstructures of the specimens (a) YSZ and (b) YSZ/Ni sintered at 1600 °C in CO. Arrows indicate the Ni particles.

observed at the right shoulder of every peak in Fig. 5(c). The hump is resulted from the Kα2 reflection [18]. The cubic phase is also found in the YSZ specimen sintered at 1400 °C in CO, and its major phase is the first tetragonal (t) phase. As the sintering temperature increases to 1500 °C, t phase is no longer existed. The second tetragonal phase, t′, is observed instead. Furthermore, the amount of c phase is too low to be detected. The t′ phase is also found on the surface region of the YSZ specimen sintered at 1600 °C in CO. Nevertheless, the first tetragonal phase, t phase, is found along with a small amount of the c phase in the interior of the specimen. The XRD pattern of the YSZ/Ni composite is very similar to that of the YSZ specimen prepared by sintering in CO. It demonstrates that the addition of Ni particles has little influence on the phase transition of zirconia. The lattice parameters of the tetragonal phases, t and t′ phases, are shown in Table 1. These values are close to the reported lattice parameters for the t and t′ phases [17].

4. Discussion

4.1. Phase transition

The major phase for the YSZ specimens sintered in air is the first tetragonal (t) phase. By increasing the sintering temperature, a small amount of c phase is observed. There is no t′-phase found in the specimens sintered in air. The formation of c phase has been related to the diffusion of Y_2O_3 from inside of the grain to its boundary [31,32]. As the Y_2O_3 segregation at the grain boundary reaches a value above ~5.7 mol%, the c phase is formed.

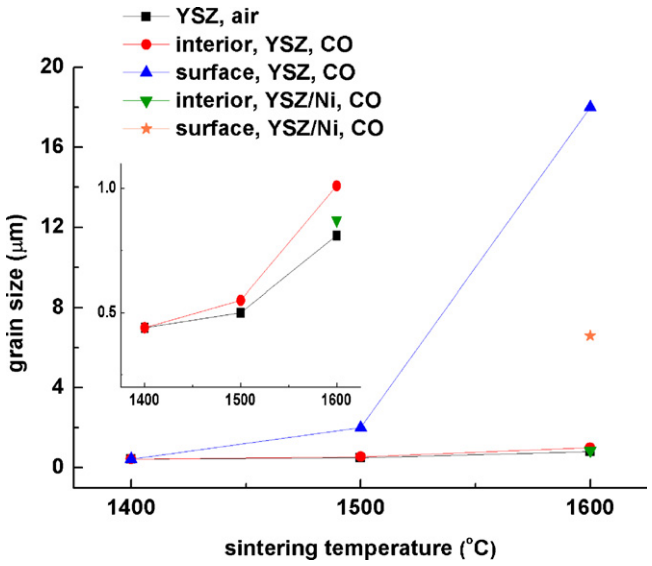

Fig. 4. Size of ZrO_2 grains as function of sintering temperature.

As the YSZ specimens are sintered above 1450 °C in the reducing atmosphere produced by the graphite powder bed, a second tetragonal (t′) phase is observed. The t′ phase is found only in the surface region of the specimens. The presence of t′ phase was first reported by Miller [12]. He proposed that the formation of t′ phase is resulted from the diffusionless shear transformation from cubic phase. He suggested that a fast cooling process was needed in order to produce t′ phase. Though t′ phase was also termed as un-equilibrium tetragonal phase [10], Cheng and Thompson suggested that t′ phase would not transform to monoclinic phase under an external load [15]. In the present study, a relatively slow cooling rate, 5 °C/min, was used. Furthermore, the specimens were covered with a graphite powder in a covered crucible. A even slower cooling rate is resulted. Furthermore, the t′-phase is formed only at the surface of the specimens, Fig. 5(c), t-phase remains within the specimen.

After sintering the YSZ specimen at 1400 °C in the reducing atmosphere for 1 h, the major phase is still the first tetragonal phase. The density of specimen is ~5.7 g/cm^3, corresponding to a relative density around 94%. Most the pores at such density are isolated to the outer environment. As the sintering temperature further increases to above 1450 °C, the phase of the surface region starts to transform from t to t′. The phase within the specimen remains the same. The amount of c-phase is below the detection limit of the present XRD technique employed. It suggests that the formation of t′-phase is not likely through the diffusionless transformation from c to t′, but more likely through a diffusion-assisted transformation.

The formation of cubic phase can be achieved by adding aliovalent oxides. For example, the increase of Y_2O_3 addition increases the oxygen vacancy as demonstrated in the following Eq. (1):

$$Y_2O_3 \xrightarrow{ZrO_2} 2Y_{Zr}' + V_0^{\bullet\bullet} + 3O_x \quad (1)$$

The above reaction suggests that the oxygen vacancy content increases with the increase of Y_2O_3 content. The cubic phase is formed as Y_2O_3 content reaches 5.7 mol% [31,32]. The

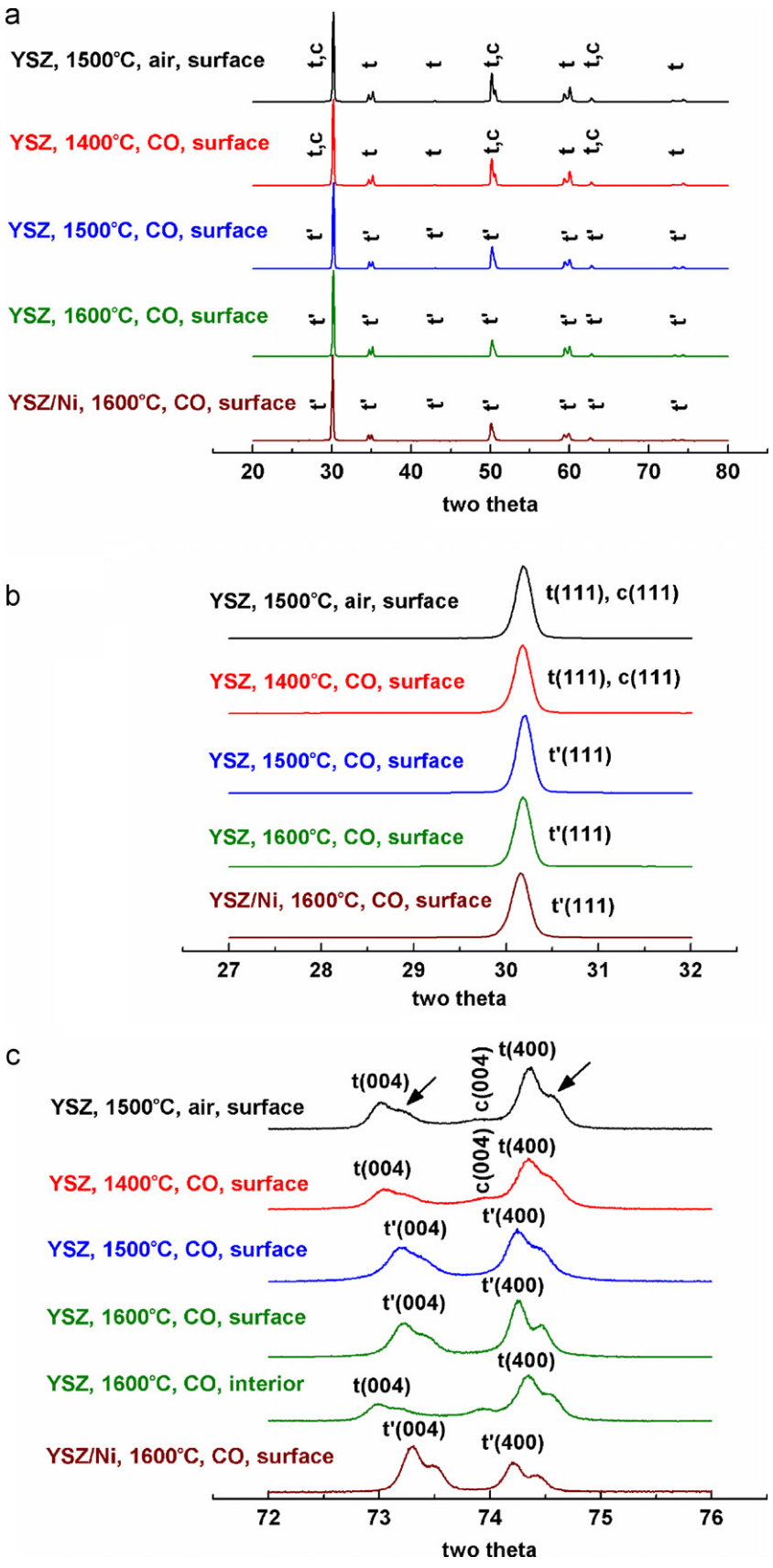

Fig. 5. XRD patterns in the 2θ range from (a) 20° to 80°, (b) 27° to 32° and (c) 72° to 76°. Arrows indicate the Kα2 shoulder.

Table 1
Tetragonal phases and their lattice parameters as calculated from Fig. 5(c).

Specimens	Analyzed location	Phase	c (Å)	a (Å)	c/a ratio
YSZ, 1500 °C/air	Surface	t	5.179	5.098	1.016
YSZ, 1400 °C/CO	Surface	t	5.178	5.099	1.015
YSZ, 1500 °C/CO	Surface	t′	5.168	5.105	1.012
YSZ, 1600 °C/CO	Surface	t′	5.166	5.104	1.012
YSZ, 1600 °C/CO	Interior	t	5.181	5.099	1.016
YSZ + 0.5 vol% Ni, 1600 °C/CO	surface	t′	5.162	5.107	1.011

concentration of Y_2O_3 as a function of location is analyzed by using EPMA technique. The results are shown in Table 2. No noticeable difference in the Y_2O_3 concentration between surface and interior of YSZ specimens is found. The EPMA analysis suggests that the formation of t′-phase is not assisted through the re-distribution of Y_2O_3.

Apart from the addition of aliovalent oxides, to fire the specimen in an environment of low oxygen partial pressure can also produce oxygen vacancy as demonstrated in the following reaction,

$$O_0 \rightarrow \tfrac{1}{2}O_2 + V_0^{\bullet\bullet} + 2e' \quad (2)$$

The t′ phase is found only at the surface region of the specimens after firing above 1450 °C. The pores in the surface region are isolated to each other, Fig. 2(d). The strong correlation between the formation of vacancy and t′ phase, suggesting that the t′ phase is likely formed through the formation of oxygen vacancy during firing in the reducing atmosphere. Through the diffusion of oxygen vacancy into the interior of specimen, the t′ phase grows into the specimen.

Though the transformation ability of t′ to m is far from clear yet, several previous works claimed that t′ phase is stable against external load [19,33]. Nevertheless, the phase transformation from t′ to m has also been reported [34,35]. For the YSZ specimen prepared by sintering at 1600 °C in CO, there is around 5–10% t′ transformed to m phase after surface grinding with a diamond wheel (not shown here). A volume expansion is accompanied with the transformation. Cracks are thus observed in the surface region after grinding, see Fig. 2(d). It suggests that t′-phase can transform to m-phase as an external load is applied. The grain size of t′-phase prepared in the present study is >20 μm, which is much larger than the values reported in the previous studies [13,17]. The transformation ability of the t′-phase prepared in the present study may be related to its large grain size. An in-depth investigation into the effect of grain size on the transformation ability of t′-phase is needed.

Table 2
Yttria concentration at surface and interior of the YSZ specimens. The specimens were sintered in CO at the indicated temperatures for 1 h.

	Yttria concentration/mol%		
	1400 °C	1500 °C	1600 °C
Surface	3.07 ± 0.09	2.98 ± 0.27	2.82 ± 0.37
Interior	3.09 ± 0.08	3.24 ± 0.12	2.90 ± 0.33

4.2. Grain growth behaviour

The grain growth behaviour of tetragonal (t) phase during sintering above 1300 °C in air had been investigated [26,31,32,36]. A high Y^{3+} segregation within a 10 nm region near grain boundary has been confirmed through a microstructure analysis [31,32]. The grain growth of t-phase in air is sluggish, due to the grain boundary is dragged by the Y^{3+} solutes.

For the YSZ specimens sintered in CO at elevated temperature, the grain growth rate in the surface region starts to pick up as the sintering temperature is above 1500 °C. The increase of the grain growth rate corresponds closely to the formation of t′ phase. From Figs. 2(d) and 3(a), the size of the grains decreases with the increase of the distance from the surface. The pores in the surface region mainly locate at the triple junctions. The trapped pores, the pore separated from the grain boundaries, are hardly observed. Furthermore, the size of the pores also decreases with the increase of the distance from the surface. It indicates that the grain growth behaviour of the t′ phase is a typical pore-dragging type [37].

Previous studies indicated that the grain growth rate of cubic phase is much faster than that of tetragonal phase [27]. In the present study, the fast grain growth rate is found only when the t′-phase is formed. In terms of the c/a ratio, Table 1, the crystal structure of t′ phase is more symmetrical than that of t phase. The grain growth rate of the t′ phase is thus expected to be faster than that of the t phase.

The grains at the surface region of the YSZ specimens sintered at 1600 °C in CO are large. It allows us to estimate the Y_2O_3 concentration at the grain boundary of the coarse grains by using the EPMA technique. The results for are shown in Table 3. No Y_2O_3 segregation at grain boundary is noted. The Y_2O_3 content distribution for the specimen sintered at 1500 °C in CO has also been determined. No difference in Y_2O_3 content

Table 3
Yttria concentration of the surface region for the YSZ specimen sintered at 1600 °C in CO for 1 h.

	Yttria concentration/mol%
Grain boundary region	2.98 ± 0.07
Grain region	2.87 ± 0.20

between large grains and small grains has been observed. It again confirms that the fast grain growth rate is not contributed by the re-distribution of Y_2O_3, but related to the increase of oxygen vacancy and subsequently the formation of t′ phase. A strong correlation between the grain growth behaviour and formation of t′ phase is observed.

The t′ phase remains stable (without grinding) even when the grain size of t′ phase is larger than 20 μm. Though the addition of Ni particles has little influence on the phase transformation from t to t′. The addition of nickel particles slows down the movement of grain boundaries. The role of Ni particles is similar to that of pores, they drag the grain boundaries to slow the grain growth rate.

5. Conclusions

The use of graphite powder bed affects the phase and microstructure of YSZ specimen. In the present study, a new formation mechanism for the second tetragonal phase, t′, is proposed. The t′-phase is transformed from t-phase as YSZ is sintered in a reducing atmosphere above 1450 °C. The formation of t′-phase is assisted by the increase of oxygen vacancies. The grain growth rate of t′ zirconia is very fast; coarse t′ grains are thus formed on the surface region. Though the t′ grains can be larger than 20 μm, no m-phase is observed after cooling from elevated temperature. The growth of t′ ZrO_2 grains is contributed by a pore dragging process. The Ni particles can also drag the grain boundaries; the size of the ZrO_2 grains in the YSZ/Ni composite is therefore smaller.

References

[1] Y.Q. Wang, G. Sayre, Commercial thermal barrier coatings with a double-layer bond coat on turbine vanes and the process repeatability, Surf. Coat. Technol. 203 (2009) 2186–2192.

[2] S.M. Haile, Fuel cell materials components, Acta Mater. 51 (2003) 5981–6000.

[3] Z. Mutasim, W. Brentnall, Thermal barrier coatings for industrial gas.

[4] J. Maček, B. Novosel, M. Marinšek, Ni-YSZ SOFC anodes−minimization of carbon deposition, J. Eur. Ceram. Soc. 27 (2007) 487–491.

[5] T. Kim, G. Liu, M. Boaro, S.-I. Lee, J.M. Vohs, R.J. Gorte, O.H. Al-Madhi, B.O. Dabbousi, A study of carbon formation and prevention in hydrocarbon-fueled SOFC, J. Power Sources 155 (2006) 231–238.

[6] V.A. Restrepo, J.M. Hill, Carbon deposition on Ni/YSZ anodes exposed to CO/H2 feeds, J. Power Sources 195 (2010) 1344–1351.

[7] R.H.J. Hannink, P.M. Kelly, B.C. Muddle, Transformation toughening in zirconia-cantaining ceramics, J. Am. Ceram. Soc. 83 (3) (2000) 461–487.

[8] J.M. Leger, P.E. Tomaszewski, A. Atouf, A.S. Pereira, Pressure-induced structural phase transitions in zirconia under high pressure, Phys. Rev. B 47 (1993) 14075–14083.

[9] J. Kondoh, Origin of the hump on the left shoulder of the X-ray diffraction peaks observed in Y2O3-fully and partially stabilized ZrO2, J. Alloys Compd. 375 (2004) 270–282.

[10] A.H. Heuer, R. Chaim, V. Lanteri, The displacive cubic→tetragonal transformation in ZrO2 alloys, Acta Metall. 35 (3) (1987) 661–666.

[11] T.B. Cheng, D.P. Thompson, Nitrogen-containing tetragonal zirconia, J. Am. Ceram. Soc. 74 (5) (1991) 1135–1138.

[12] R.A. Miller, J.L. Smielek, R.G. Garlick, Phase stability in plasma-sprayed partially stabilized zirconia-yttria, Advances in Ceramics, in: A.H. Heuer, L.W. Hobbs (Eds.), Science and Technology of Zirconia, vol. 3, American Ceramic Society, Columbus, OH, 1981, pp. 241–253.

[13] A.H. Heuer, R. Chaim, V. Lanteri, Review: phase transformations and microstructural characterization of alloys in the system Y_2O_3–ZrO_2, in: S. Somiya, N. Yamamoto, H. Yanagida (Eds.), Advances in Ceramics, Science and Technology of Zirconia II, vol. 24A, American Ceramic Society, Westerville, OH, 1986, pp. 3–20.

[14] V. Lanteri, R. Chaim, A.H. Heuer, On the microstructures resulting from the diffusionless cubic→tetragonal transformation in Y2O3-ZrO2 alloys, J. Am. Ceram. Soc. 69 (10) (1986) C-258–C-261.

[15] Y. Cheng, D.P. Thompson, The transformability of tetragonal ZrO2 in some glass systems, J. Mater. Sci. Lett. 9 (1) (1990) 24–27.

[16] J. Chevalier, L. Gremillard, A.V. Virkar, D.R. Clarke, The tetragonal-monoclinic transformation in zirconia: lessons learned and future trends, J. Am. Ceram. Soc. 92 (9) (2009) 1901–1920.

[17] W.Z. Zhu, T.C. Lei, Y. Zhou, Z.S. Ding, Ageing behaviour of t′-phase in a hot-pressed ZrO_2(4 mol% Y_2O_3) ceramic, J. Mater. Sci. 30 (1995) 6235–6242.

[18] A. Paterson, R. Stevens, Phase analysis of sintered yttria-zirconia ceramics by X-ray diffraction, J. Mater. Res. 1 (2) (1986) 295–299.

[19] T.J. Chung, H. Song, G.H. Kim, D.Y. Kim, Microsturcture and phase stability of yttria-doped tetragonal zirconia polycrystals heat treated nitrogen atmosphere, J. Am. Ceram. Soc. 80 (10) (1997) 2607–2612.

[20] M.V.G. Pirovano, A.H.J. Sauer, Oxygen vacancies in transition metal and rare earth oxides: current state of understanding and remaining challenges, Surf. Sci. Rep. 62 (2007) 219–270.

[21] Y.K. Paek, J.H. Ahn, G.H. Kim, S.J. Kang, Effect of nitrogen atmosphere on the densification of a 3-mol%-yttria-doped zirconia, J. Am. Ceram. Soc. 85 (2002) 1631–1633.

[22] Y.B. Cheng, D.P. Thompson, Role of anion vacancies in nitrogen-stabilized zirconia, J. Am. Ceram. Soc. 76 (3) (1993) 683–688.

[23] M. Matsuzawa, M. Abe, S. Horibe, J. Sakai, The effect of reduction on the mechanical properties of CeO_2 doped tetragonal zirconia ceramics, Acta Mater. 52 (2004) 1675–1682.

[24] N. Mommer, T. Lee, J.A. Gardner, Stability of monoclinic and tetragonal zirconia at low oxygen partial pressure, J. Mater. Res. 15 (2) (2000) 377–381.

[25] F.F. Lange, Transformation toughening. 3. Experimental-observations in the ZrO_2-Y_2O_3 system, J. Mater. Sci. 17 (1982) 240–246.

[26] J. Chevalier, S. Deville, E. Münch, R. Jullian, F. Lair, Critical effect of cubic phase on aging in 3mol% yttria-stabilized zirconia ceramics for hip replacement prosthesis, Biomaterials 25 (2004) 5539–5545.

[27] J.A. Allemann, B. Michel, H.B. Marki, L.J. Gauckler, E.M. Moser, Grain-growth of differently doped zirconia, J. Eur. Ceram. Soc. 15 (1995) 951–958.

[28] M.P. Harmer, H.M. Chan, G.A. Miller, Unique opportunities for microstructural engineering with duplex and laminar ceramic composites, J. Am. Ceram. Soc. 75 (7) (1992) 1715–1728.

[29] F. Esteban-Betegón, S. Lopez-Esteban, J. Requena, C. Pecharromán, J.S. Moya, Obtaining Ni nanoparticles on 3Y-TZP powder from nickel salts, J. Am. Ceram. Soc. 89 (1) (2006) 144–150.

[30] D.R. Gaskell, Introduction to the Thermodynamics of Materials, 3 ed, Taylor & Francis, New York, 1995.

[31] K. Matsui, H. Horikoshi, N. Ohmichi, M. Ohgai, Cubic-formation and grain-growth mechanism in tetragonal zirconia polycrystal, J. Am. Ceram. Soc. 86 (8) (2003) 1401–1408.

[32] K. Matsui, H. Yoshida, Y. Ikuhara, Phase-transformation and grain-growth kinetics in yttria-stabilized zirconia polycrystal doped with a small amount of alumina, J. Eur. Ceram. Soc. 30 (7) (2010) 1679–1690.

[33] J.F. Jue, A.V. Virkar, Fabrication, microstructural characterization, and mechanical properties of polycrystalline t′-zirconia, J, Am. Ceram. Soc. 73 (12) (1990) 3650–3657.

[34] J.F. Jue, J. Chen, A.V. Virkar, Low-temperature ageing of t′-zirconia: the role of microstructure on phase stability, J. Am. Ceram. Soc. 74 (8) (1991) 1811–1820.

[35] B. Liang, C. Ding, H. Liao, C. Coddet, Study in structural evolution of nanostructured 3 mol% yttria stabilized zirconia coatings during low temperature ageing, J. Eur. Ceram. Soc. 29 (2009) 2267–2273.

[36] J. Zhao, Y. Ikuhara, T. Sakuma, Grain growth silica-added zirconia annealed in the cubic/tetragonal two-phase region, J. Am. Ceram. Soc. 81 (8) (1998) 2087–2092.

[37] R.J. Brook, Pore-grain boundary interactions and grain growth, J. Am. Ceram. Soc. 52 (1) (1969) 56–60.